

Crack risk analysis in structural elements exposed to hygrothermal phenomena

A. Meda

University of Rome "Tor Vergata", Italy

G. Plizzari & C. Zanotti

University of Brescia, Italy

S. Cangiano

CTG-Italcementi Group, Bergamo, Italy

ABSTRACT: Past experiences showed that some concrete constructions are significantly affected by the risk of cracking a short time after casting, due to hygrothermal phenomena (that is to say shrinkage, hydration heat development and temperature variations of the surroundings). The problem of hygrothermal cracking is getting more and more significant due to the introduction in practice of High Strength Concrete, having a high cement content. A numerical study on shrinkage cracking in concrete walls is presented in this paper. Aim of the analysis is to assess the influence of different factors, such as the degree of restraint between the wall and the foundation slab, the amount of both ordinary longitudinal and transverse reinforcement and the addition of fibers in the concrete mix. Two main crack indicators are adopted: the maximum crack opening along the whole structure and the global crack pattern.

1 INTRODUCTION

Hygrothermal phenomena in concrete, i.e. shrinkage, hydration heat or ambient thermal, can be cause of cracking and thus jeopardize both structure performance and durability. It is well known that those phenomena produce strains that may induce stresses and, as a consequence, cracking. Hygrothermal cracking typically involves constructions having particular features such as large size, low thickness or high degree of restraint.

Shrinkage of concrete mainly consists of volume changes induced by both evaporation and movement of water. Internal and external restraints (provided, for example, by adjacent structural elements or steel reinforcement), contrasting shrinkage deformations, provoke tensile stresses that can cause cracking. Massive structures such as concrete walls are particularly exposed to the risk of shrinkage cracking, which is further favored in the case of elements having a low thickness. From a structural point of view, similar effects are involved by thermal variations of the surroundings.

Nonlinear FE analyses of the cracking process in concrete walls undergoing time-dependent volume changes are presented herein. The main aim of the research is to determine different representative levels of damage and then assess the corresponding

limit values of allowable volume changes. To this purpose, two main indicators of damage are adopted: the maximum crack opening along the whole structure and the global crack pattern. Concrete cracking is modeled by means of a smeared approach, combined to a multi-directional fixed crack model. The influence of many factors, such as geometry, longitudinal reinforcement (which provides an internal restraint thus favoring cracking, but, at the same time, counteracts the crack opening) and transverse reinforcement (which weakens the concrete section and, as a consequence, significantly favors the first cracking), is evaluated. Furthermore, different degrees of restraint between the wall and the foundation slab are considered by adopting interface elements which model both the tangential slip and the normal detachment.

2 CASE STUDY

The case study presented herein is a concrete wall having a length of 30 m and a cross section of 5 x 0.5 m (Fig. 1). The wall is considered as placed on a foundation slab, resting on sand soil and having a width of 1.5 m and a thickness of 0.5 m (Fig. 1). The structure undergoes the dead load and the volume changes that are induced by concrete shrinkage.

Shrinkage stresses may be caused by external or internal constraints provided by soil and longitudinal steel reinforcement, which counteract the contraction of concrete elements. The crack risk in the present structure is especially influenced by differential shrinkage between the wall and the foundation slab. In fact, the foundation slab is commonly cast some days before the wall and thus the foundation shrinkage is partly developed when the wall is cast. Differential shrinkage is further increased by the actual difference between the two geometries; in fact, drying shrinkage, which is caused by water evaporation, is strongly affected by both shape and size of concrete elements (ACI 2005).

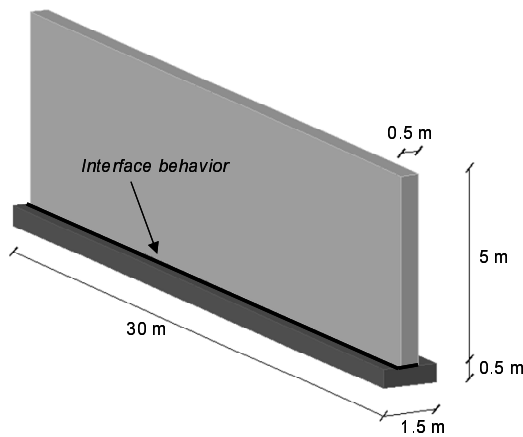


Figure 1. Reference geometry.

It is well known that the tensile behavior of cracked concrete can be significantly enhanced by fibers, which are able to efficiently sew micro-cracks and thus increase concrete toughness (Romualdi & Batson 1963, Shah & Rangan 1971, di Prisco et al. 2004, Van Mier 2004, Gettu 2008).

In order to assess the influence of fibers on shrinkage cracking, the responses of plain concrete and Fiber Reinforced Concrete (FRC) walls are compared herein. Hooked steel fibers, having a length (l) of 50 mm, a diameter (d) of 1 mm (aspect ratio $l/d = 50$), are adopted; the fiber volume fraction (V_f) is 0.38%, corresponding to a fiber content of 30 kg/m³.

As a longitudinal reinforcement, two steel rebars are placed every 250 mm along the wall height. Three different diameters, ϕ , corresponding to different reinforcement ratios, ρ_s , are adopted: (i) $\phi = 6$ mm and $\rho_s = 0.048\%$, (ii) $\phi = 8$ mm and $\rho_s = 0.13\%$, (iii) $\phi = 10$ mm and $\rho_s = 0.26\%$. Stirrups with two legs, a diameter of 10 mm and a spacing of 250 mm, are adopted. For the foundation, six longitudinal rebars, having a diameter of 10 mm are placed on top and bottom.

Finally, different degrees of restraint between the wall and the foundation, depending on the interface properties, are considered.

For the numerical simulations, a normal strength concrete C30/37 (EC2 2004) is considered.

3 FE MODELING

Transient nonlinear numerical analyses are performed by means of Diana FE program (release 9.2, de Witte & Kikstra 2005a).

As the structure is doubly symmetrical, just a quarter of the whole geometry is represented. Differential shrinkage between the wall and the foundation is simulated by applying strains that are uniformly distributed along the wall and increase with time.

No-tension translational springs are applied at the bottom of the foundation slab for modeling sand soil. Winkler elastic soil is assumed having a stiffness $k_w = 90 \times 10^6$ N/m³ and is represented by no-tension springs placed in the FE nodes present at the bottom surface of the foundation; each spring has a stiffness that is a function of the corresponding area of soil. According to the results of a preliminary study, the degree of restraint provided by soil friction is negligible in comparison with the constraint provided by the foundation slab, which counteracts the wall contraction (Plizzari et al. 2009); therefore, soil friction is here neglected.

3.1 Plain concrete and FRC

Concrete parts are modeled by means of cubic linear-strain isoparametric elements, having size of 125x125x125 mm. For both elastic modulus and tensile strength, reference is made to the European standards (EC2 2005).

Concrete cracking is modeled by means of the smeared approach, combined to the multi-directional fixed crack model (Rots 1988). The nonlinear tension softening suggested by Cornelissen et al. (1986) is adopted for plain concrete, as shown in Figure 2; fracture energy, G_f , is determined by reference to the CEB-FIP Model Code 90 (1993). Fiber Reinforced Concrete is modeled as a homogeneous material, whose mechanical properties are provided by the experimental work of Cominoli et al. (2005); a simplified bi-linear law represents the tension softening behavior of FRC (Fig. 2). Provided that low compressive stresses are involved, a linear elastic behavior is assumed for concrete under compression.

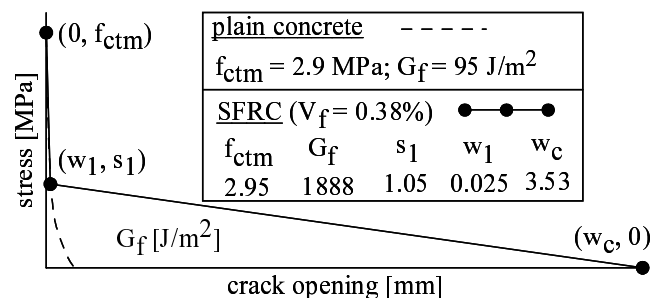


Figure 2. Tension softening laws for plain concrete (Cornelissen et al. 1986, CEB-FIP Model Code 1990) and Fiber Reinforced Concrete (Cominoli et al. 2005, Zanotti et al. 2009).

3.2 Ordinary steel reinforcement

Besides the well-known benefits, ordinary steel reinforcement may induce secondary negative effects in concrete elements subjected to significant shrinkage. Since shrinkage strains mainly develop along the longitudinal axis of the long wall analyzed in the present paper (Fig. 1), longitudinal steel rebars provide internal constraint, while stirrups laying along the transverse axis weaken the resistant concrete section.

The longitudinal reinforcement of the wall is modeled by means of truss elements, which are able to simulate also the internal constraint counteracting concrete shrinkage strains. Differently, embedded reinforcement is adopted for the foundation slab. A symmetrical elasto-plastic behavior, with a hardening branch after yielding, is assumed for steel under tensile and compressive stresses (Fig. 3).

Modeling of volumes taken up by stirrups would require a very fine mesh, incompatible with the wall size. Therefore, in order to account for the section weakening as well as the stress concentration provided by transverse reinforcement, tensile strength of elements that should contain stirrups is properly decreased. To this aim, local tensile tests along directions perpendicular to the stirrup axis were preliminary simulated by means of numerical analyses and the mechanical properties of a new equivalent material were thus determined (Plizzari et al. 2009).

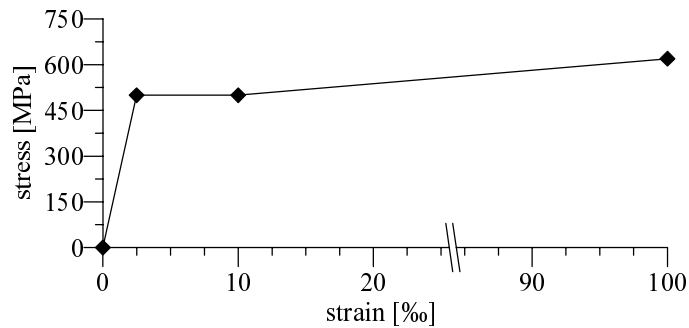


Figure 3. Behavior of steel under tension or compression.

3.3 Wall-foundation interface behavior

The surface shared by the wall and the foundation slab is modeled by means of 16-nodes interface elements, having zero-thickness (that is normal length $l_n = 0$) and tangential dimensions l_t equal to 125 mm.

Material properties are defined as functions between tangential or normal stresses and the corresponding relative displacements of the element nodes (de Witte & Kikstra 2005b). Hence, the elastic normal stiffness, D_{11} , is given by Equation (1):

$$D_{11} = \frac{t_n}{\Delta u_n} = \frac{E}{l_n} \approx \frac{E}{10^{-4} l_t} \approx \frac{E}{10^{-5} \text{ m}} = 3.3 \cdot 10^{15} \frac{\text{N}}{\text{m}^3} \quad (1)$$

where t_n = average normal stress; Δu_n = relative displacement in normal direction; and E = concrete elastic modulus, equal to 3.3 GPa in the case of concrete class C30/37 (EC2 2005). Please note that Equation 1 is based on the hypothesis that the infinitesimal thickness l_n is four orders of magnitude lower than the tangential length l_t .

Both displacements and strains are assumed small in the elastic field, as shown by Equations (2), (3), for determining the elastic tangential stiffness, D_{22} :

$$G = \frac{t_t}{\gamma} = t_t \frac{l_n}{\Delta u_t} \quad (2)$$

$$D_{22} = \frac{t_t}{\Delta u_t} = \frac{G}{l_n} = \frac{D_{11}}{2(1+\nu)} = 1.375 \cdot 10^{15} \frac{\text{N}}{\text{m}^3} \quad (3)$$

where t_t = average tangential stress; Δu_t = relative displacement in tangential direction; γ = shear rate; G = shear modulus; and ν = Poisson coefficient (typically assumed 0.2 for concrete). In order to assess the accuracy of those stiffness values, that is, to verify the compatibility between the stiffness of concrete bricks and interface elements, numerical local tests in both normal and tangential directions were performed (Plizzari et al. 2009).

The nonlinear interface behavior is modeled by means of Mohr-Coulomb law. Two different surface types are considered: smooth and rough interface. The smooth surface is representative of a situation with a very low degree of restraint between the wall and the foundation; conversely, a high degree of restraint is provided by the rough cast joint. Finally, the maximum restraint condition is considered by assuming perfect bond between the two structural elements; either slips or detachments are not allowed in that case.

The interface properties, listed in Table 1, are derived from the parameters suggested by the European standards (EC2 2005) for cast joints. The tensile strength of the cast joint is $f_{t,int} = c/\tan\phi$, where c is the cohesion coefficient and ϕ is the friction coefficient. Tension softening is neglected at the interface. Associated plasticity is assumed.

Table 1. Parameters defining the nonlinear interface behavior.

Surface type	c [MPa]	ϕ	$f_{t,int}$ [MPa]
smooth	1.305	26.5°	1.45
rough	1.725	35°	1.86

c = cohesion coefficient

ϕ = friction angle

$f_{t,int}$ = tensile strength of the cast joint

4 DISCUSSION OF THE FE RESULTS

4.1 Elastic stress distribution

Figure 4 shows the qualitative distribution of elastic longitudinal stresses (σ_z) in the case of perfect bond between wall and foundation. Boundary effects involve a length of $L_B = 10$ m. Numerical analyses performed for varying the wall height confirmed that $L_B = 2H$, as a general rule, with H the wall height (Plizzari et al. 2009).

Critical points, that are the points affected by the maximum tensile stresses, are close to the lateral edges, due to boundary effects, and lay in the bottom part of the wall, at a height $h_c = t/2$ (where t is the wall thickness), due to the high degree of restraint developed in that area.

Figures 5, 6 show, respectively, the stress distribution along the longitudinal and vertical axes passing through the critical point, just before cracking. As expected, the major contribution is provided by longitudinal stresses. Please note that stresses are remarkably nonlinear due to the relevant wall height (Nilsson 2003). Furthermore, the inversion of longitudinal stresses can be observed at 2.5-3 m from the foundation; the upper part of the wall is therefore affected by compressive stresses (ACI 1995).

4.2 Crack pattern development for ordinary RC walls

Crack patterns of ordinary concrete walls without reinforcement, obtained for different degrees of restraint with the foundation slab, are compared in Figure 7; the lower the degree of restraint, the lower the wall cracking. Regardless of the wall-foundation interface properties, first cracking occurs for shrinkage strains equal to $125 \cdot 10^{-6}$. Immediately after cracking, strains localize along two vertical macro-cracks due to the lack of both ordinary steel reinforcement and/or fibers.

Interface properties mainly affect local micro-cracking, which is significant with perfect bond (Fig. 7a). Conversely, with a smooth interface (low friction), a minor local micro-cracking affects the boundaries (Fig. 7c).

Regardless of the interface properties and the reinforcement ratio, first cracking of RC walls occurs with a shrinkage strain $\epsilon = 48.7 \cdot 10^{-6}$. In comparison with walls without reinforcement, first cracking of RC walls occurs earlier due to the section weakening provided by stirrups.

The main phases of a RC wall cracking can be observed in Figure 8; cracks appear and develop along the concrete parts that are weakened by stirrups; furthermore, diffused cracking occurs at the bottom interface. The crack pattern development can be divided in the following phases: 1) first cracking occurs at

boundaries, in the lower part of the wall, 2) micro-cracks spread to the middle of the wall; 3) cracks grow in vertical direction; and 4) principal cracks localize (first at boundaries and then, in the middle).

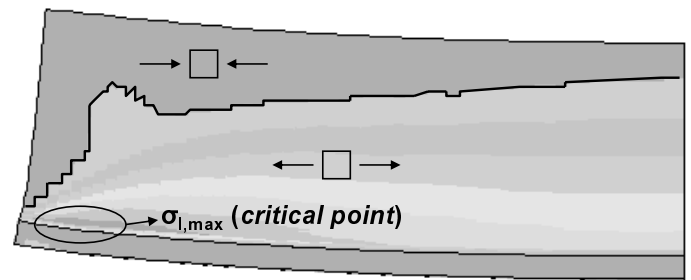


Figure 4. Elastic distribution of longitudinal stresses.

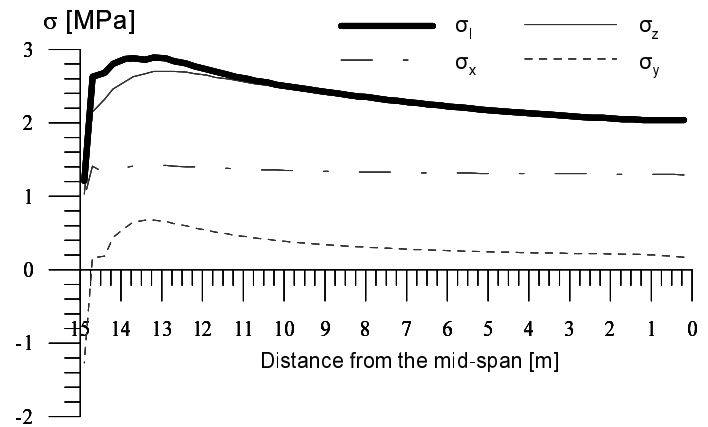


Figure 5. Elastic stress distribution along the longitudinal axis passing through the critical point (Fig. 4) just before cracking: maximum principal stress σ_I and longitudinal, vertical and transverse stresses (σ_z , σ_y , σ_x , respectively).

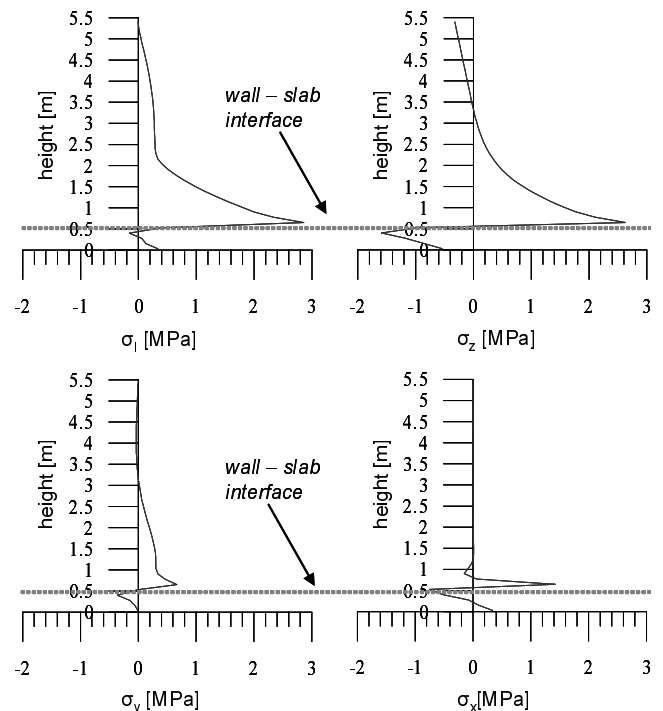


Figure 6. Elastic stress distribution along the vertical axis passing through the critical point just before cracking: maximum principal stress σ_I and longitudinal, vertical and transverse stresses (σ_z , σ_y , σ_x , respectively).

4.3 Influence of longitudinal rebars on crack patterns

The diagram of Figure 9 shows the maximum crack openings that are reached in the structure for increasing shrinkage volume changes for a rough wall-foundation interface. The results obtained when varying the longitudinal reinforcement ratio ρ_s are compared. Benefits provided by longitudinal reinforcement are clearly visible: the higher the amount of reinforcement, the smaller the maximum crack opening corresponding to a given value of shrinkage volume changes. As an instance, a crack opening of 0.5 mm is reached when shrinkage strains equal $135 \cdot 10^{-6}$ with the lowest reinforcement ratio, and $145 \cdot 10^{-6}$ in the other cases. The influence of steel rebars on the crack opening increases for increasing shrinkage strains; as a matter of fact, a crack opening of 0.8 mm is associated to volume changes equal to $135 \cdot 10^{-6}$, $150 \cdot 10^{-6}$, or $210 \cdot 10^{-6}$, depending on the reinforcement ratio.

Provided that longitudinal rebars do not affect first cracking and enhance crack patterns at the whole, it may be finally deduced that the internal restraint effect is negligible, compared with the restraint provided by the foundation slab.

Three different crack levels may be identified:

- 1st level: cracks spread along the wall base (strongly affected by both stirrups and wall-foundation interface properties);
- 2nd level: localized vertical cracks that do not reach the top of the wall;

- 3rd level: vertical cracks covering the whole height.

The different branches of the “maximum crack opening vs. volume changes” curves correspond to different stages of the wall cracking, that are numbered in Figure 9 and can be summarized as follows:

1) Micro-cracking, spread along the wall base (1st level).

2) Formation of the first vertical macro-crack (2nd level, Fig. 10) and strain localization, followed by a sudden increment of the maximum crack opening.

3) Development of other vertical macro-cracks (2nd level, Fig. 11); in this stage, the increase of volume changes is followed by multiple-cracking, without increase of the maximum crack opening, as an advantage provided by steel rebars.

4) A vertical crack reaches the top of the wall at each half (3rd level); as a result, the wall is essentially subdivided in three parts that are not bonded to each other.

5) Primary macro-cracks develop (3rd level). With the highest reinforcement ratio, a further vertical crack develops at this stage (Fig. 12); as a consequence, primary cracks open less than in the other cases.

6) In the wall having the highest reinforcement ratio, strains localize around the new vertical crack (point 5). Accordingly, primary cracks are partially closed and the maximum crack opening suddenly decreases up to 0.6 mm. Later on, the crack opening starts increasing again and reaches values of 0.8-1 mm for volume changes that are significantly higher than in the other cases.



Figure 7. Crack patterns of the concrete wall with no reinforcement, in the case of perfect bond between wall and foundation (a), and rough (b) or smooth (c) interface.

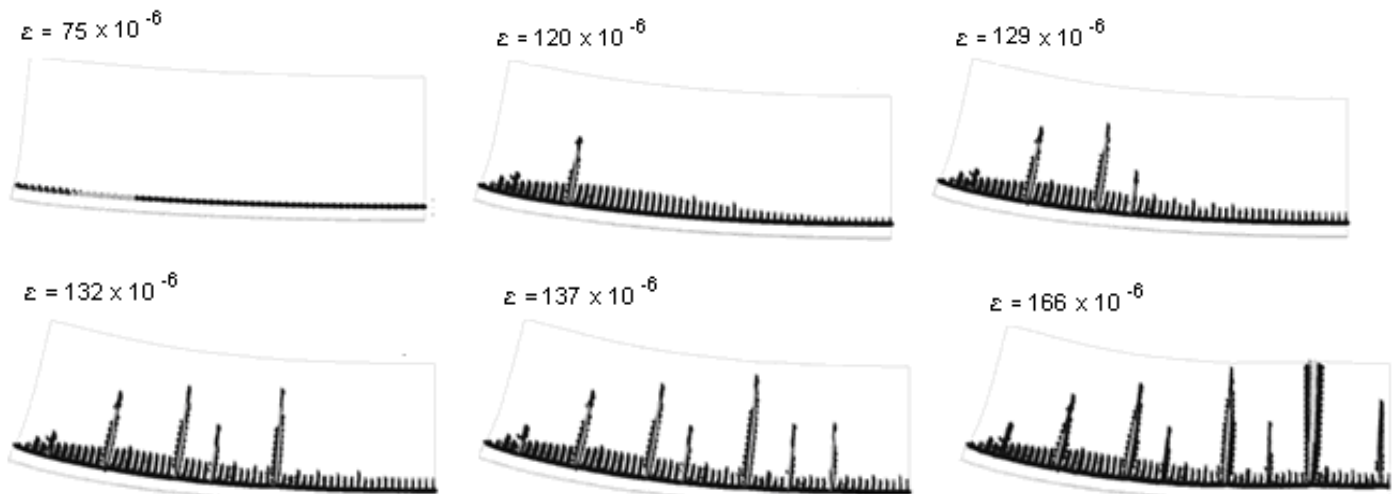


Figure 8. Development of the crack pattern for increasing shrinkage strains (ϵ), in the case of wall reinforcement ratio $\rho_s = 0.13\%$ and rough wall-foundation interface.

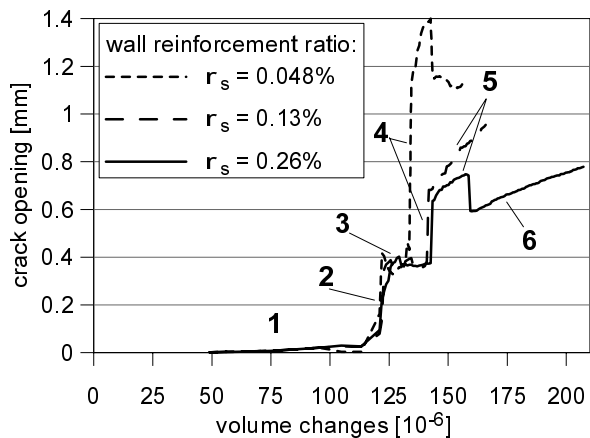


Figure 9. Maximum crack opening obtained for increasing shrinkage volume changes in the wall, in the case of rough wall-foundation interface.

4.4 Influence of the wall-foundation interface properties on crack patterns

In diagrams of Figures 13, 14, responses of walls having the same amount of longitudinal reinforcement, but different degrees of restraint with the foundation slab (that is to say different wall-foundation interface properties), are compared. On the whole, higher structure performances are achieved in the case of smooth wall-foundation interface than in the case with more friction. As a matter of fact, a friction reduction causes a crack opening reduction.

The influence of the wall-foundation interface on crack patterns is particularly significant in the case with $\rho_s = 0.048\%$, that is the lowest reinforcement ratio (Fig. 13). Conversely, the role of the interface roughness is secondary for higher values of ρ_s , since in those cases steel rebars are anyway able to effectively limit the crack opening.

4.5 Influence of the wall geometry on crack patterns

In Figure 15 the “maximum crack opening-vs. shrinkage volume changes” curves obtained by varying the wall geometry are compared. Besides the reference geometry, having height $H = 5$ m and length $L = 6H = 30$ m, two more cases are considered: one with a height equals to half the reference height ($H = 2.5$ m and $L = 12H = 30$ m) and the other one having a length equal to $2/3$ the reference length ($H = 5$ m and $L = 4H = 20$ m). The corresponding crack patterns are shown in Figures 16, 17. By reducing the ratio L/H , the structure performance is enhanced. L/H can be reduced by reducing L (for instance, by placing proper vertical joints) or by increasing H . The height increase provides a secondary further benefit, which is the reduction of the constraint provided by the foundation slab, due to the increment of the ratio between the cross areas of the wall and the foundation (Cusson & Repette 2000).

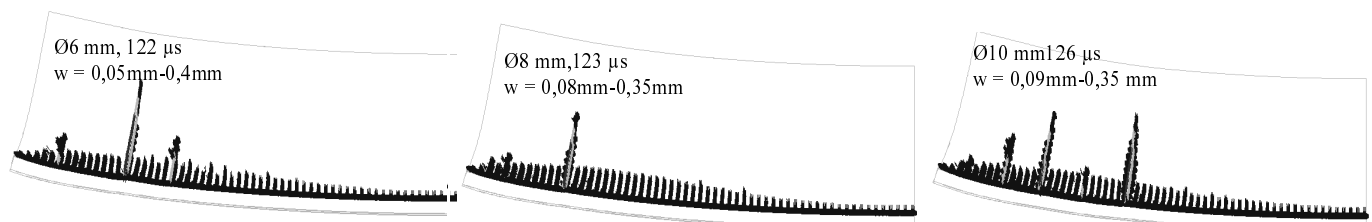


Figure 10. Crack patterns corresponding to the occurrence of the first vertical macro-crack (point 2, Fig. 9), obtained for varying the diameter of longitudinal rebars, that is to say the wall reinforcement ratio.

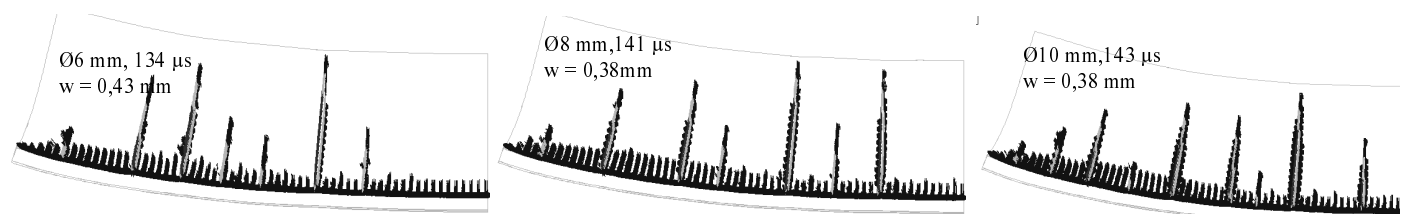


Figure 11. Crack patterns corresponding to point 3 of Figure 9, obtained for varying the diameter of longitudinal rebars, that is to say the wall reinforcement ratio.

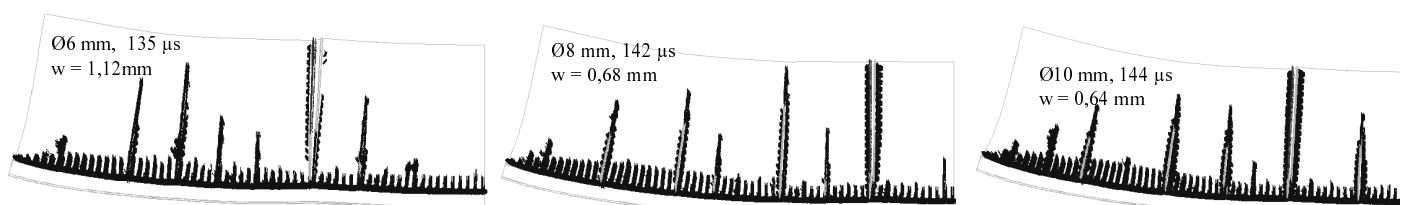


Figure 12. Crack patterns corresponding to the macro-crack localization (point 4, Fig. 9), obtained for varying the diameter of longitudinal rebars, that is to say the wall reinforcement ratio.

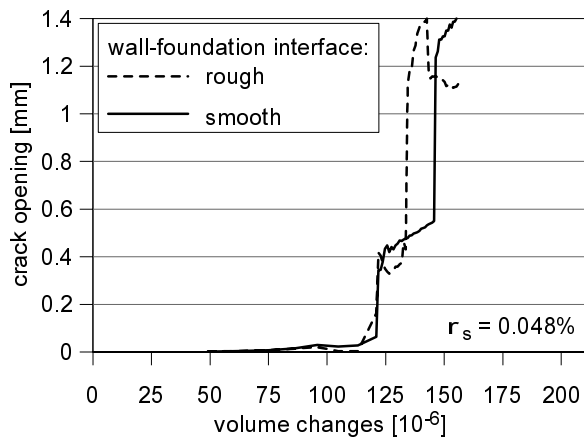


Figure 13. Maximum crack opening obtained for increasing shrinkage volume changes in the wall having a reinforcement ratio $\rho_s = 0.048\%$.

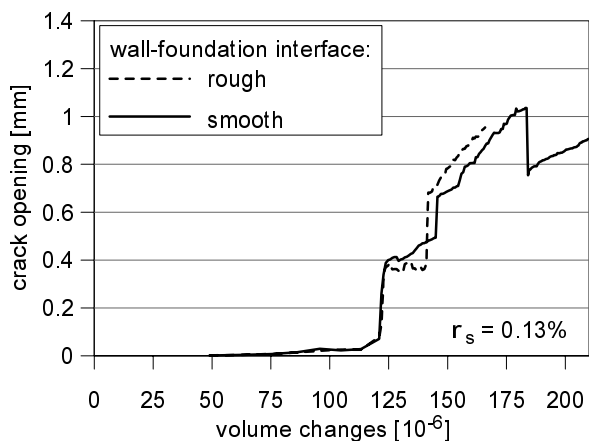


Figure 14. Maximum crack opening obtained for increasing shrinkage volume changes in the wall having a reinforcement ratio $\rho_s = 0.13\%$.

In the wall having $L/H = 12$ (Fig. 16), a larger number of primary vertical cracks (3^{rd} level), with a spacing almost equal to the wall height, can develop in comparison with the other two cases. As a matter of fact, lower vertical stresses are involved and, in the central part of the structure, no compressive longitudinal stress develops. Conversely, boundary effects are unchanged. In the case with the reference height of 5 m and a reduced length ($L = 4H = 20$ m), the influence of vertical compressive stresses is emphasized so that no primary cracks appear (Fig. 17). Longitudinal stresses are more remarkably non linear and boundary effects affect the whole length.

4.6 Containment of crack opening by means of fiber reinforced concrete

Diagrams plotted in Figures 9, 15 show that the structure performance can be enhanced by increasing the amount of longitudinal steel reinforcement or by placing vertical joints (in order to reduce L/H). However, those solutions turn out to be effective only in the large deformation field, for limiting crack openings larger than almost 0.3 mm. A smeared reinforcement - such as fibers - may be added to the concrete mix in order to enhance the

material toughness (Fig. 2) and, therefore, to better control also micro-cracking. Figure 18 allows to compare responses of a wall reinforced by means of ordinary steel rebars ($\rho_s = 0.13\%$, curve 1) and a wall reinforced by means of hooked steel fibers ($V_f = 0.38\%$ as afore described, curve 2). The results evidence fiber capabilities in controlling the micro-crack opening, unlike conventional rebars, which effectively work only for larger deformations. Finally, an optimized solution for designing the reinforcement with respect to shrinkage effects could be achieved by properly combining fibers and conventional rebars. Therefore, the behavior of a FRC wall reinforced with steel rebars only at the top is analyzed, provided that the maximum opening of primary cracks occurs in the upper part of the structure. The results show that the performance of the FRC wall in the large deformation field can be improved by means of longitudinal rebars placed at the top, since the crack opening is further reduced (curve 3, Fig. 18).

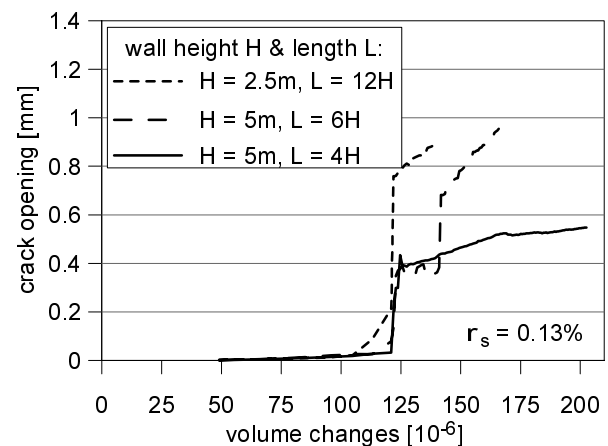


Figure 15. Maximum crack opening obtained for increasing shrinkage volume changes in the wall having a reinforcement ratio $\rho_s = 0.13\%$, a rough wall-foundation interface and a variable geometry.

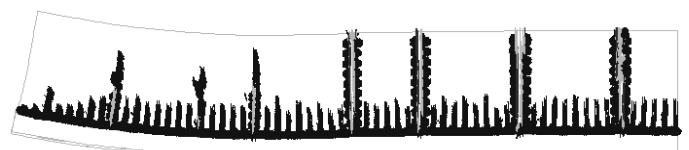


Figure 16. Crack pattern of the wall having height $H = 2.5$ m and length $L = 12H = 30$ m.

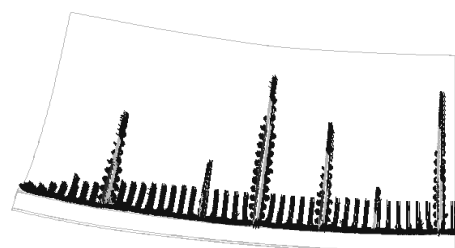


Figure 17. Crack pattern of the wall having height $H = 5$ m and length $L = 4H = 20$ m.

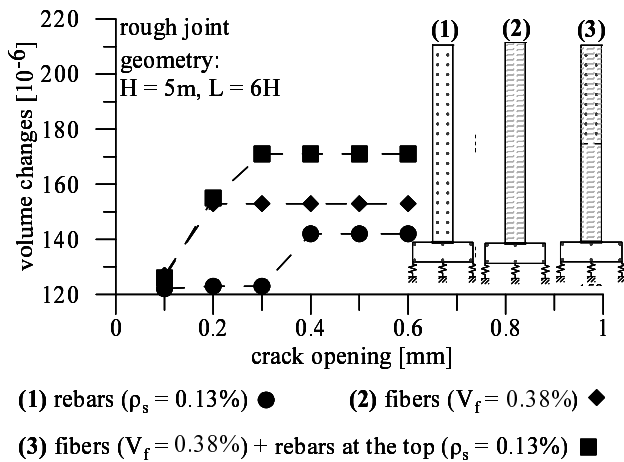


Figure 18. Response of walls reinforced by means of conventional rebars (curve 1), hooked steel fibers (curve 2) or an optimized combination of fibers and rebars (curve 3).

5 CONCLUDING REMARKS

A nonlinear numerical study on shrinkage cracking in R/C walls was presented. The major results discussed herein can be summarized as follows:

- The restraint provided by the slab foundation is the main cause of stresses that develop in the wall undergoing concrete shrinkage.
- The cracking onset occurs along the bottom, in the areas close to the lateral edges of the wall, due to boundary effects.
- The degree of restraint between the wall and the slab foundation, that is to say the interface roughness, affects the development of cracks localized at the bottom as well as the openings of primary vertical cracks; the interfacial roughness effect is significant, most of all, in the case of low content of longitudinal reinforcement.
- Longitudinal steel reinforcement improves the whole structure behavior; as a matter of fact, longitudinal rebars favor multiple cracking and limit the crack opening. Conversely, the internal restraint effect turns out to be negligible.
- Transverse reinforcement weakens the concrete section and thus significantly anticipate first cracking; moreover, cracking at the bottom is strongly increased.
- Longitudinal rebars are not effective in controlling crack openings lower than 0.3 mm; conversely, micro-cracks can be effectively limited by means of fiber reinforcement.
- An optimized reinforcement, obtained by properly combining steel rebars and fibers, can be adopted for limiting shrinkage cracking.

REFERENCES

- ACI 1995. Effect of restraint, volume change and reinforcement on cracking of mass concrete (ACI 207.2R-95). American Concrete Institute.
- ACI 2005. Report on factors affecting shrinkage and creep of hardened concrete (ACI 224.1R-05). American Concrete Institute.
- CEB-FIP Model Code 1990, Comité Euro-International du Béton.
- Cominoli, L., Meda, A., Plizzari, G. 2005. Hybrid fibers to enhance fracture properties of concrete pavements. In Proc. of the Third Int. Conf. on Construction Materials, Vancouver, Canada.
- Cornelissen, H.A.W., Hordijk, D.A., Reinhardt, H.W. 1986. Experimental determination of crack softening characteristics of normalweight and lightweight concrete. Heron 31,2.
- Cusson, D. & Repette, W. 2000. Early-age cracking in reconstructed bridge barrier walls. ACI Materials Journal, July-August, pp. 438-446.
- de Witte, F.C. & Kikstra W.P. 2005a. DIANA – Finite Element Analysis. User's manual release 9. Analysis Procedures. Delft: TNO DIANA BV
- de Witte, F.C. & Kikstra W.P. 2005b. DIANA – Finite Element Analysis. User's manual release 9. Material Library. Delft: TNO DIANA BV
- di Prisco, M., Felicetti, R., Plizzari, G.A. 2004. Proceedings of the 6th RILEM Symposium on Fiber Reinforced Concretes (FRC), BEFIB-2004, Varenna (Italy), 20-22 September, RILEM PRO 39, Bagnaux (France): 1514 pp.
- EC2 2005. Design of concrete structures. Part 1-1: General rules and rules for buildings. EN 1992-1-1.
- Gettu, R. 2008. Proceedings of the Seventh Intl. RILEM Symp. on Fibre Reinforced Concrete: Design and Applications, BEFIB-2008, 17-19 September, pp. 1154.
- Nilsson, M. 2003. Restraint factors and partial coefficient for crack risk analyses of early age concrete structures. Doctoral thesis. Luleå University of Technology.
- Plizzari, G., Meda, A., Zanotti, C. 2009. Studio numerico sul rischio di prematura fessurazione delle opere in calcestruzzo. Technical Report, Università degli Studi di Brescia, Dipartimento DICATA. In press. In Italian.
- Romualdi, J.P., Batson, G.B 1963. Mechanics of crack arrest in concrete beam with closely spaced reinforcement. Journal of the American Institute, 60, pp. 775-789.
- Rots, J.C 1988. Computational modeling of concrete fracture. Doctoral thesis. Delft University of Technology (NL).
- Shah, S.P. & Rangan, B.V. 1971. Fibre reinforced concrete properties. ACI Journal Proceedings, 68(2), pp. 126-134.
- Van Mier, J.G.M. 2004. Cementitious composites with high tensile strength and ductility through hybrid fibres. In Proc. of the 6th RILEM Symposium on Fibre Reinforced Concrete, BEFIB-2004, Varenna, Lake Como, Italy, 20-22 September, 2004.
- Zanotti, C., Cangiano, S., Meda, A., Plizzari, G. 2009. Problematiche legate al rischio di prematura fessurazione delle opere in calcestruzzo. In Proc. of the AICAP Conference, Pisa, 14-16 May 2009. In Italian.